Results in Physics 12 (2019) 989–995

Contents lists available at ScienceDirect

Results in Physics

journal homepage: www.elsevier.com/locate/rinp

Eco-friendly synthesis of Fe_3O_4 nanoparticles: Evaluation of their catalytic activity in methylene blue degradation by kinetic adsorption models

Álvaro de Jesús Ruíz-Baltazar[a,*], Simón Yobanny Reyes-López[b,*], María de Lourdes Mondragón-Sánchez[c], Anel Ivonne Robles-Cortés[c], Ramiro Pérez[d]

[a] CONACYT-Centro de Física Aplicada y Tecnología Avanzada, Universidad Nacional Autónoma de México, Boulevard Juriquilla 3001, Santiago de Querétaro, Querétaro C.P. 76230, Mexico

[b] Instituto de Ciencias Biomédicas, Universidad Autónoma de Ciudad Juárez, Estocolmo s/n, Ciudad Juárez, Chihuahua C.P. 32300, Mexico

[c] Tecnológico Nacional de México/Instituto Tecnológico de Morelia, Posgrado en Metalúrgia, Av. Tecnológico 1500, col, Lomas de Santiaguito, C.P. 58120 Morelia, MICH, Mexico

[d] Instituto de Ciencias Físicas, Universidad Nacional Autónoma de México, Av. Universidad s/n, Col. Chamilpa, Cuernavaca, MOR 62210, Mexico

ARTICLE INFO

Keywords:
Green synthesis
Fe_3O_4 nanoparticles
Kinetic adsorption models
Methylene blue degradation

ABSTRACT

In this work the green synthesis of Fe_3O_4 nanoparticles by *cynara cardunculus* leaf extract is presented. This green synthesis route offers a novel and eco-friendly alternative to obtaining of iron oxides nanoparticles. Functional nanoparticles with potential catalytic applications, particularly for water remediation containing organic dyes were synthetized. The structural characterization of the Fe_3O_4 nanoparticles were carried out by scanning electron microscopy (SEM), X-ray diffraction, techniques. Calculation to obtaining the crystallite size by Williamson –Hall method were performed. Additionally, Raman spectroscopy support the Fe_3O_4 characterization. Posteriorly, the Fe_3O_4 nanoparticles were evaluated on the methylene blue degradation. Kinetic adsorption models were employed to establish the behavior during the methylene blue degradation process. Pseudo first order, Pseudo second order, Intraparticle diffusion and Elovich Models were calculated based on the experimental data obtained. Calculations as the correlation factor indicates the best linear fit between the theoretical models and the experimental data obtained during the blue methylene degradation.

Introduction

In recent years, the development of nanomaterials has aroused much interest due to the potential application in multiple fields such as physics, chemistry, biomedicine, optics, electronics and catalysis, among other [1–4]. The reason why these nanomaterials have motivated several studies, is due to the remarkable properties that are exhibited, such as their high thermal and electrical conductivity, their demonstrated catalytic activity and their biocompatibility [5–8]. In this sense, the optimization of the morphology and distribution of the size of the materials, conditions the mentioned properties. In the specifically case of the iron oxide nanoparticles, many synthesis methodologies as hydrothermal, solvothermal, electrothermal and co-precipitation method has been reported [9–12], in this methodologies, factor as the temperature, PH, concentration of the surfactant and reducing agents. However, this lasted mentioned are generally toxic and in general represent high costs to carry out the synthesis process. For this reason, the search for the development of new alternative synthesis routes, respectful of the environment, non-expensive and non-toxic, represents a nodal challenge in the development of new nanomaterials [13–17]. In the case of the magnetite nanoparticles has been widely studied due to their magnetic, catalytic and biocompatibility properties [18]. The iron oxide nanoparticles have been employed as vectors for drug, magnetic resonance imaging contrast agents, for adsorption of antibiotics and heavy metal and degradation of organic dyes [19,20]. The degradation of organic pollutants from water can be focused in clean energy sources [10,21]. For this reason in nowadays the study of the catalytic properties of the oxides iron nanoparticles has attached much interest. In this sense, this work focuses on the attention to this problem through functional alternatives, which represent a low cost and friendly to the environment.

Many plants extracts have been employed and reported for the synthesis of Fe_3O_4 NPs, however, the proposed methodology is simple, economic and has not been reported [22,23]. On the other hand, Cynara cardunculus has multiple therapeutic and alimentary applications due to their great quantity of antioxidants presents in this plant [24]. In

* Corresponding authors.
E-mail addresses: aruizbaltazar@fata.unam.mx (Á.d.J. Ruíz-Baltazar), simon.reyes@uacj.mx (S.Y. Reyes-López).

https://doi.org/10.1016/j.rinp.2018.12.037
Received 23 October 2018; Received in revised form 4 December 2018; Accepted 8 December 2018
Available online 20 December 2018

this sense, the abundance and particular properties of this species allow affirming that the Cynara cardunculus take an important role on the economic development on their cultive zones [25]. For this reason, the green synthesis of the Fe_3O4 nanoparticles by sustainable material as artichoke can be considered as a functional methodology for obtaining nanoparticles of iron oxides and a novel research.

In this work, the green synthesis route to obtain Fe_3O_4 nanoparticles is presented. This route is based in a reduction of the iron using *cynara cardunculus* leaf extract. This eco-friendly methodology offer a facile synthesis at low cost and non-toxic alternative to obtaining magnetic materials. The structural and spectroscopic characterization by Scanning Electron Microscopy (SEM), X-ray diffraction (XRD) and Raman spectroscopy is presented. In terms of the properties evaluation, the methylene blue degradation by the Fe_3O_4 nanoparticles were studied by UV–vis spectroscopy. Kinetics adsorption models were performed to establish the behavior during the methylene blue degradation process. Pseudo first order, Pseudo second order, Intraparticle diffusion and Elovich Models were calculated based on the experimental data obtained. Calculations as the correlation factor indicates the best linear fit between the theoretical models and the experimental data obtained during the blue methylene degradation.

Experimental procedure

Bio-synthesis of Fe_3O_4 nanoparticles

The Fe3O4 nanostructures were synthesis starting to a mixture of ferric chloride and ferrous chloride in a 1:2 M ratio. The reducing agent employed was *cynara cardunculus* leaf extract with voucher specimen number 260583. The plant was obtained from Tarímbaro City, Mex. Briefly, a solution of [Fe (III)/Fe (II)] in aqueous solution at 50 mM was prepared in aqueous solution. On other hand, 5 gr of dried leaves of cynara cardunculus was milled and transferred to a 50 ml flask with 30 ml of deionized water. The cynara cardunculus was heated to 100 °C for 20 min. The infusion obtained was cooled at room temperature and mixed whit 20 ml of [Fe (III)/Fe (II)] solution (50 mM). The PH associated with the reaction was adjusted to 11 through a solution of NaOH. A color change of the post-reaction mixtures from dark brown into black color was observed. This coloration change indicate the iron oxide formation.

Methylene blue degradation

The catalytic activity analysis of Fe_3O_4 NPs was carried out through the degradation of MB. The experiments were performed employed 3 mg of Fe_3O_4 NPs synthesized *cynara cardunculus* leaf extract. The initial concentration of MB was 30 mgL^{-1}. The MB degradation process was monitored by UV–vis in intervals of 5 min until the SPR of the organic dye disappeared.

Results and discussions

Scanning Electron Microscopy (SEM)

Fig. 1(a) shows the Fe_3O_4 nanoparticles obtained by green synthesis using cynara cardunculus leaf extract. In this image we can appreciated the Scanning Electron Microscopy (SEM) obtained by detection of secondary electrons (SE). The morphology observed is semi-spherical, several agglomerates can be appreciated. Several studies [2,26,27] describes this agglomeration as a stearic effect attributed to the interaction of the actives sites of the NPs surface. However, the magnetic interaction generated by the individuals Fe_3O_4 nanoparticles is considerate to explain this agglomeration observed by SEM. In order to establish the chemical composition of the nanoparticles, Fig. 1(b) display an EDS spectrum of the sample, the main components observed were Fe and O. Initially, the chemical composition is consistent with the synthesis of the Fe_3O_4 nanoparticles. The particle size of the Fe_3O_4 nanoparticles is not possible to determine only by the SEM technique, in this case, it is necessary to make measurements from the X-ray Diffraction pattern from which we can calculate the crystallite size using the Scherrer equation and the Williamson-Hall (W-H) method. This analysis is presented in the X-ray characterization section presented below.

X-ray diffraction

Additionally, the structural characterization of the sample is fundamental to support the structure of the obtained nanoparticles. Fig. 2 shows an X-ray diffraction (XRD) pattern of the Fe_3O_4 NPs. Based on the intensities observed in the experimental X-Ray pattern, the symmetry associated was the structure of the Fe_3O_4 (Fm3m-325) according to the JCPDF# 96-900-5813. In order to calculate the crystallite size and strain, The Williamson-Hall method were carried out. Table 1 describe also the needed parameters for the W-H calculations. Following, the basic principles of the Williamson-Hall method are described in general form.

Table 1 display detailed the main parameter such as the diffraction angle and their miller index for each peak identified. This result show plenary, that the structure obtained is magnetite, due that the main intensities of the experimental pattern, can be indexed whit the JCPDF# 96-900-5813. In this sense we can affirm that the reduction of the Fe ions were carried out by the reducing agents presents on the *cynara cardunculus* leaf extract. In order to calculate the crystallite size and strain, The Williamson-Hall method were carried out. Table 1 describe also the needed parameters for the W-H calculations.

Following, the basic principles of the Williamson-Hall method are described in general form.

Williamson-Hall analysis

The crystallite and strain can be calculated by Williamson-Hall method, in general form this methodology implies the instrumental broadening (β) corrected for each diffraction peak by relation:

$$\beta_{hkl}^2 = (\beta_{hkl})_{measured}^2 - (\beta_{hkl})_{instrumental}^2 \quad (1)$$

On the other hand the Debye-Scherer's equation can be employed to calculate the average nanocrystallite size, which is described following:

$$D = \frac{k\lambda}{\beta_{hkl}\cos\theta} \quad (2)$$

Complementary, has been reported that the strain induced in powders associated to the crystallite defects is calculated by:

$$\varepsilon = \frac{\beta_{hkl}}{4\ \tan\theta} \quad (3)$$

In this sense, W-H method incorporate the previous equations, given as result an expression to calculate the crystallize size and strain (Eq. (4)) from the broadening corrected and observed by the experimental X-Ray diffraction patter of Fe3O4 NPs.

$$\beta_{hkl} = \frac{k\lambda}{D\cos\theta} + 4\varepsilon\ \ \tan\theta \quad (4)$$

Simplifying the previous equation, we have:

$$\beta_{hkl}\cos\theta = \frac{k\lambda}{D} + 4\varepsilon\ \ \mathrm{sen}\theta \quad (5)$$

The above equations are known as the W-H expressions. Fig. 3 illustrate graphically, the results associated to the crystallize size and strain obtained from the Fe_3O_4 NPs synthesized by green route. The crystal size calculated was 13.5 nm.

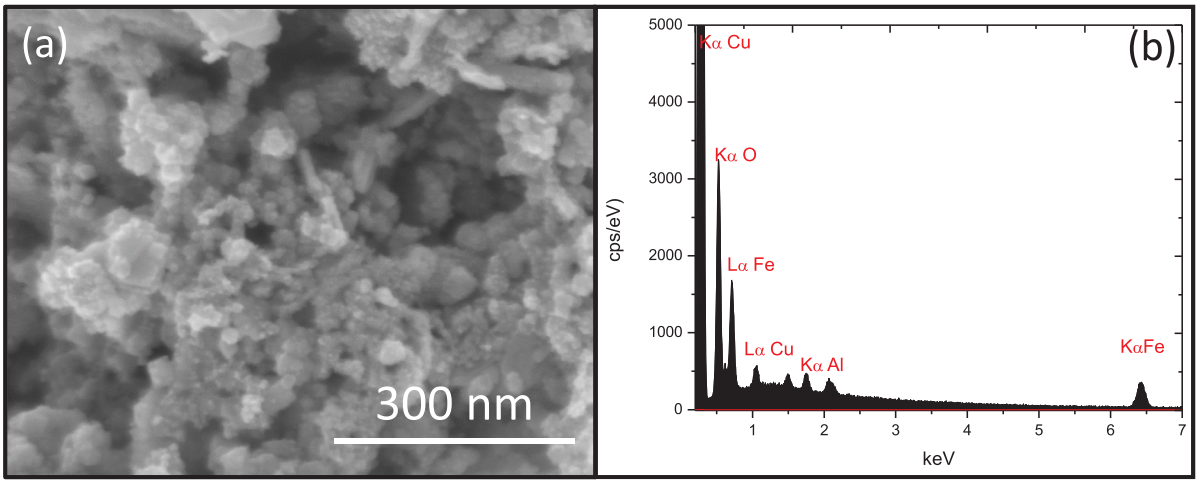

Fig. 1. (a) SEM image and (b) EDS chemical analysis of Fe3O4 nanoparticles synthesized by *cynara cardunculus* leaf extract.

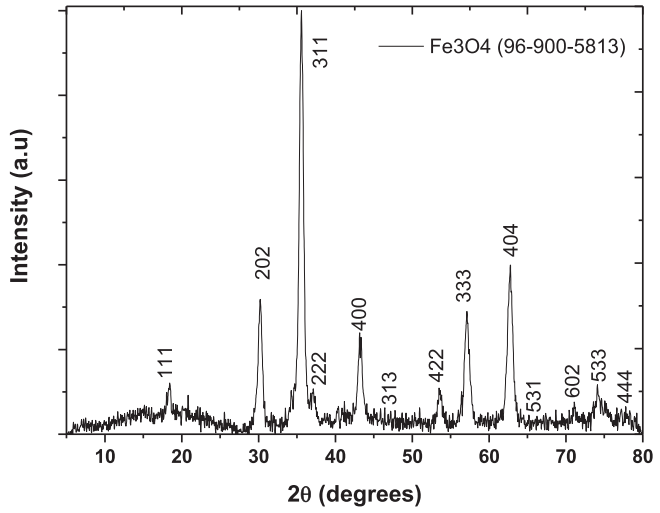

Fig. 2. X-ray diffraction (XRD) pattern of the Fe_3O_4 NPs synthesized by *cynara cardunculus*.

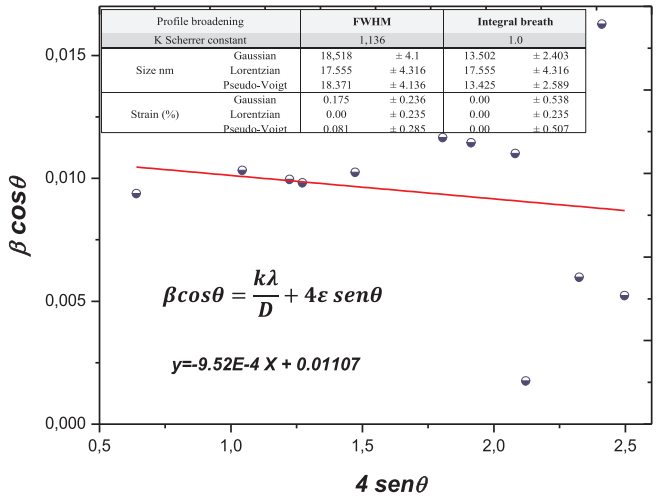

Fig. 3. Williamson-Hall plots of the Fe3O4 nanoparticles obtained by green synthesis using cynara *cardunculus* leaf extract.

Raman spectroscopy

In complementary form, the Raman spectrum of the Fe_3O_4 nanoparticles is presented in order to support the structural characterization by X-ray diffraction technique and identified the main phase present in the synthesized simple. Fig. 4 shows the Raman spectrum of the nanoparticles. Due to the magnetite possesses spinel symmetry, the expected vibrational modes of the first Brillouin zone center corresponding to this structure are given by Eq. (6) [24]:

$$\Gamma_{vib}=A_{1g} + E_{1g} + T_{1g} + 3T_{2g} + 2A_{2u} + 2E_u + 4T_{1u} + 2T_{2u} \quad (6)$$

In Fig. 4, we can identify the vibrational modes corresponding to the magnetite as principal phase. The typical vibrational mode associated to magnetite is situated t 667 cm^{-1} which is the most pronunciation

Table 1
Parameters employed for the Williamson-Hall calculations.

2θ	d-spacing (Amstrongs)	hkl	FWHM (observed)	FWHM (corrected)	Asymmetry	Areal asymmetry	Integral breadth	Shape Factor (observed FWHM/Integral breadth)	Size (nm) uncorrected	Size (nm) corrected
18.44	4.807	111	0.5474	0.544	0.4924	0.833	0.521	1.052	16.3	16.4
30.24	2.9531	220	0.6196	0.6127	0.8303	0.7458	0.772	0.803	14.8	14.9
35.62	2.5185	311	0.6083	0.5987	0.7082	0.7273	0.764	0.797	15.2	15.5
37.1	2.4213	222	0.6038	0.5932	1.2275	1.0472	0.439	1.375	15.4	15.7
43.22	2.0916	400	0.645	0.6312	0.93	1.6239	0.193	3.346	14.7	15
53.68	1.7061	422	0.7675	0.7485	0.7547	0.5042	0.634	1.12	12.9	13.2
57.16	1.6102	511	0.7687	0.7466	0.7964	0.9468	0.821	0.936	13.1	13.5
62.72	1.4802	440	0.767	0.7386	1.1993	1.0458	0.884	0.868	13.5	14
64.06	1.4524	531	0.1186	0.1186	2.7933	1.7203	0.163	0.728	87.8	87.8
71.08	1.3252	620	0.4952	0.4203	1.351	1.8582	0.331	1.498	21.9	25.8
74.14	1.2779	533	1.1959	1.1689	0.8996	0.866	1.874	1.847	9.3	9.5
77.26	1.2339	444	0.4839	0.3833	0.2629	0.408	0.398	1.217	23.3	29.5

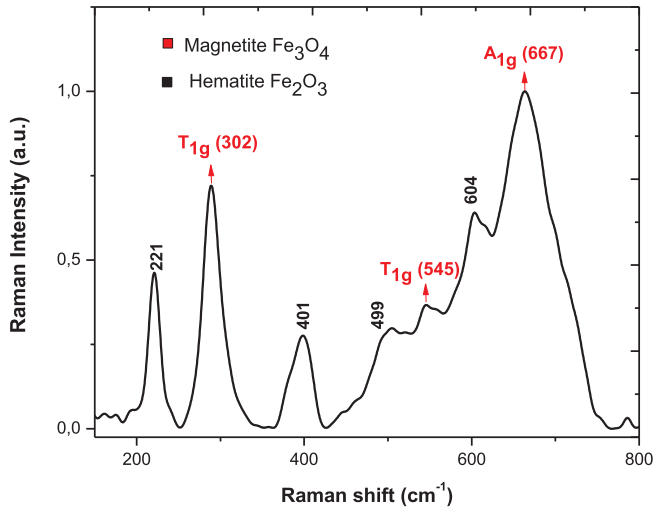

Fig. 4. Raman spectrum of the Fe_3O_4 NPs synthesized by cynara cardunculus leaf extract.

peak and correlated to the A_{1g} mode. The peaks located at 302 and 545 cm^{-1} are also representatives of the Magnetite and attributed to the T_{1g} vibrational mode [28].

Additionally, the band associated to the magnetite and hematite phases are corroborated whit Raman spectra obtained from the RRUFF Raman Mineral Spectra data base (University of Arizona). This Raman spectrum (Fig. 5a and b) indicates clearly the bans associated to the magnetite and hematite phases. Is important to note that the magnetite and hematite phases are presents in the experimental Raman spectrum, however, the majority phase observed is the magnetite. On the other hand, both phases are very similar from the point of view of the structure and the facile formation of both phases during the synthesis process is very common due to the facile interaction between the colloidal media and the iron oxide surface, promoting the oxidation of the samples. Nerveless, the green synthesis process offer a great route to obtaining magnetite NPS as majority phase, taking a count that there is not used any surfactant agent and the reducing agent employed (*cynara cardunculus* leaf extract) can be act in controlled form in comparison whit another reducing agents as for example the sodium borohydride ($NaBH_4$), which is more active in their reducing capacity and toxic [29,30]. In this sense, dispense with a surfactant agent during the green synthesis process presented, favors the reduction of the ionic iron with a suitable reaction speed for the gradual formation of iron oxide phases. Giving as a result a green and functional methodology for obtaining magnetite.

In order to elucidate the organic compound presents on the cynara cardunculus leaf extract, Fig. 6(a) shows the UV–vis spectrum of the cynara cardunculus extract. In this image we can appreciate the typical SPR of the flavonoids, which are identified by two mains bands. The band (I) is associated to the flavonols with the hydroxyl group in the ring C3 (insert Fig. 6a) [24]. Has been reported that the typical flavonol presents in the Cynara cardunculus is the quercetin. On the other hand, the band (II) is associated to the flavones. The mentioned compounds are also identified in the cynara cardunculus as the catechine among others [31]. Has been widely reported that the flavonoids exhibits a great antioxidant activity and consequently, the hydroxyl groups can favors the reduction of the iron ions given as results the magnetite formation [25]. In order to support the results obtained by UV–vis, Fig. 6(b) describe the FT-IR spectrum of the *cynara cardunculus* extract. Intensities located at 3306 cm^{-1} is attributed to the C-H stretching vibrations in the CH_2 groups identified on the aliphatic compound [25]. The bands at 1585 and 1398 and 1268 cm^{-1} are associated to the aromatics compounds such as polysaccharides [24,25]. Finally, the band observed at 1094 cm^{-1} can be associated to the aliphatic amines presents in the flavonoids identified by UV–vis spectroscopy. In this sense, the fully identifications of the organic species such as the flavonoid in the cynara cardunculus extract by UV–vis spectroscopy, allows to affirm that specifically the flavones and flavonols observed are responsible directly of the Fe ions reduction and consequently to the Fe_3O_4 NPs formation.

Theoretical adsorption kinetic models

The adsorption rate of MB observed was evaluated in terms of the four theoretical adsorption models, Pseudo first order, Pseudo second order, Elovich and intraparticle diffusion model. The first two models are expressed by Eqs. (7) and (8) [32].

$$\frac{dq}{dt} = K_1(q_e - q_t) \tag{7}$$

$$\frac{dq}{dt} = K_2(q_e - q_t)^2 \tag{8}$$

where K_1 (min^{-1}) and K_2 ($g\,mg^{-1}\,min^{-1}$) are the adsorption rate constants for pseudo first order and pseudo second order, respectively. Also, q_t and q_e represent the adsorption capacity at time t and in the equilibrium, respectively [33,34].

On the other hand, the Elovich or Roginsky and Zeldovich equation would be:

$$\frac{dq_t}{dt} = \alpha e^{-\beta q_t} \tag{9}$$

Additionally, Intraparticle Diffusion Model was employed to elucidate the MB diffusion mechanism. The kinetic equation that governs this model is [35,36]:

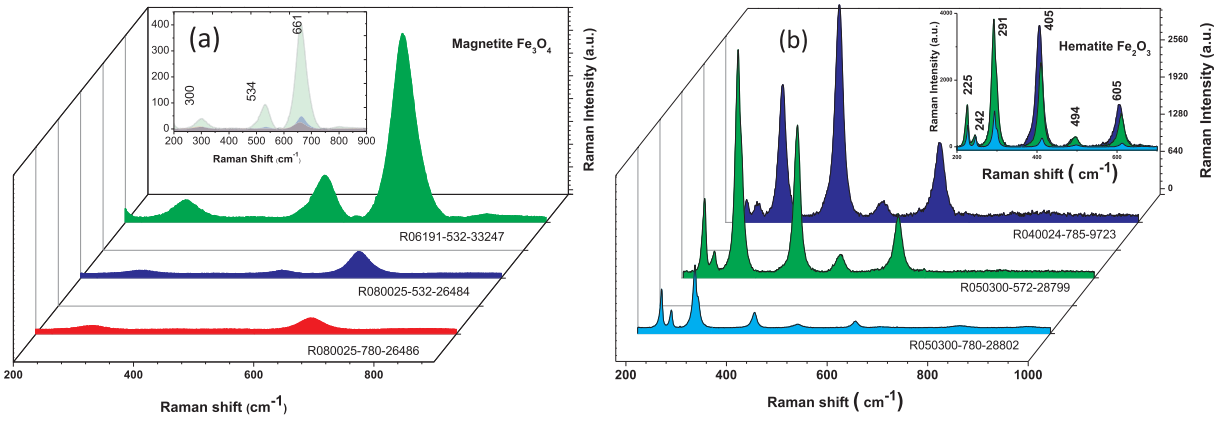

Fig. 5. Raman spectra referenced to the (a) Magnetite and (b) Hematite phases.

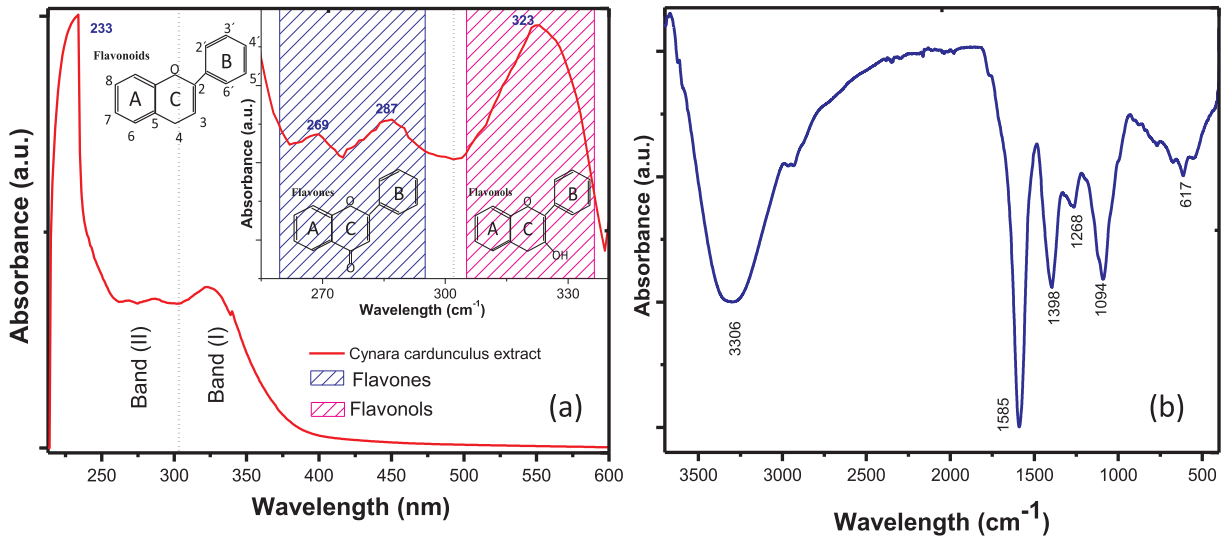

Fig. 6. (a) UV–Vis and (b) FT-IR spectra of the cynara cardunculus leaf extract employed for the green synthesis of the Fe_3O_4NPs.

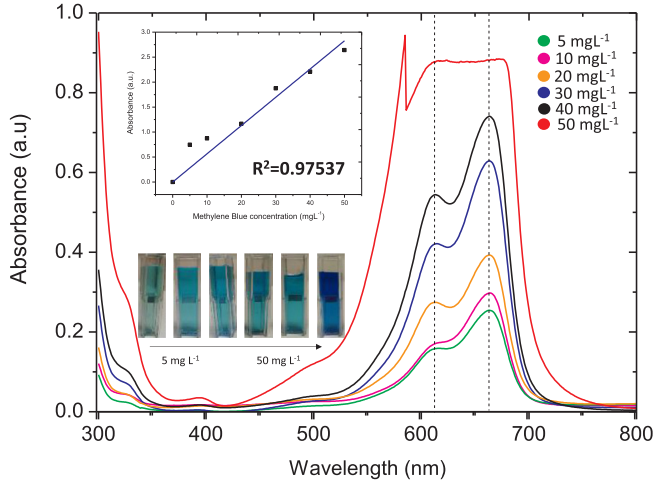

Fig. 7. Calibration curve for methylene blue absorbance in a range of 5–50 mgL^{-1}. (For interpretation of the references to color in this figure legend, the reader is referred to the web version of this article.)

$$q_t = k_i\sqrt{t} + C_i \quad (10)$$

In order to validate the MB concentration, a calibration curve of different concentration of MB solutions (5–50 g mL^{-1}) was obtained (Fig. 7). The R^2 factor observed in this linear fit is 0.9753 which can be accurate for the subsequent measurements.

Fig. 8 (a) shows the UV–vis spectrum associated to the Fe_3O_4 NPS, MB and Fe_3O_4/MB at time t = 0. In this imagen we can appreciate the typical intensity at 658 nm corresponding to the n–π* transition of MB [37]. However, the UV–Vis spectrum of the Fe_3O_4 NPs, only exhibits a low intensity at 230 nm, which can be associated to the organic compounds, which are derivate of the green synthesis of the Fe3O_4 NPS. In this sense, Fig. 8(b) shows clearly the MB degradation by the Fe_3O_4 NPS in a range of time of 80 min. The typical absorption band associated to the MB has been diminished and finally it disappeared after 80 min of reaction, which indicates that the degradation of Methylene blue dye occurs [14].

In order to evaluate the kinetic adsorption model that describes in best form the MB degradation process, Fig. 9(a)–(d) illustrate the Pseudo first and second order model, the intraparticle diffusion and Elovich model, respectively.

Based on the experimental data obtained, the linear fit of the data were obtained. The correlation factor R^2 calculated from each kinetic model, determinate the best approximation between the experimental data and the theoretical models. Table 2 indicate the kinetic parameter

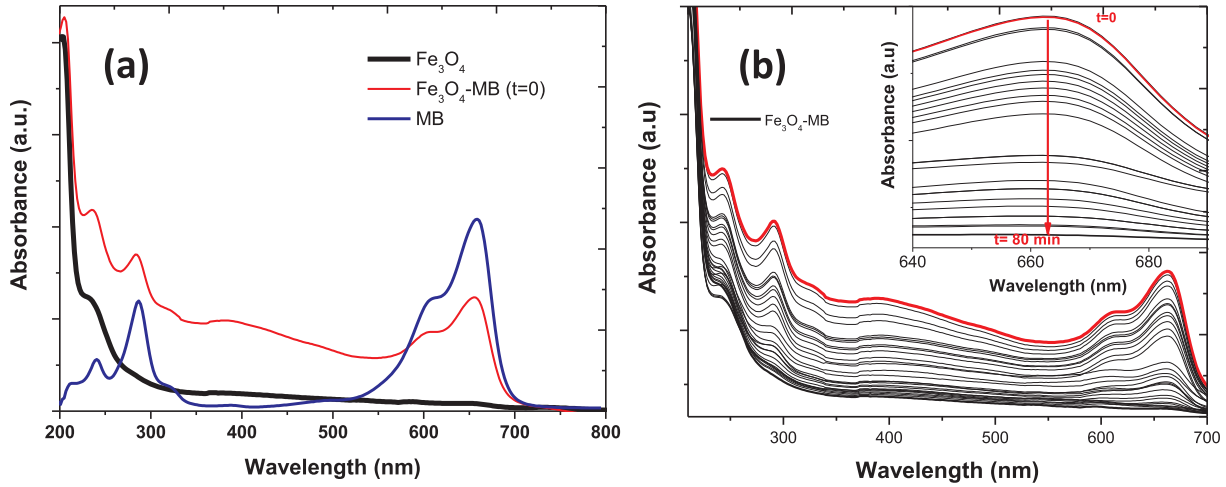

Fig. 8. (a) UV–vis spectrum of the initial samples Fe_3O_4, Fe_3O_4-MB and MB (30 mgL^{-1}), (b) Methylene blue degradation by Fe_3O_4 nanoparticles obtained by green synthesis route.

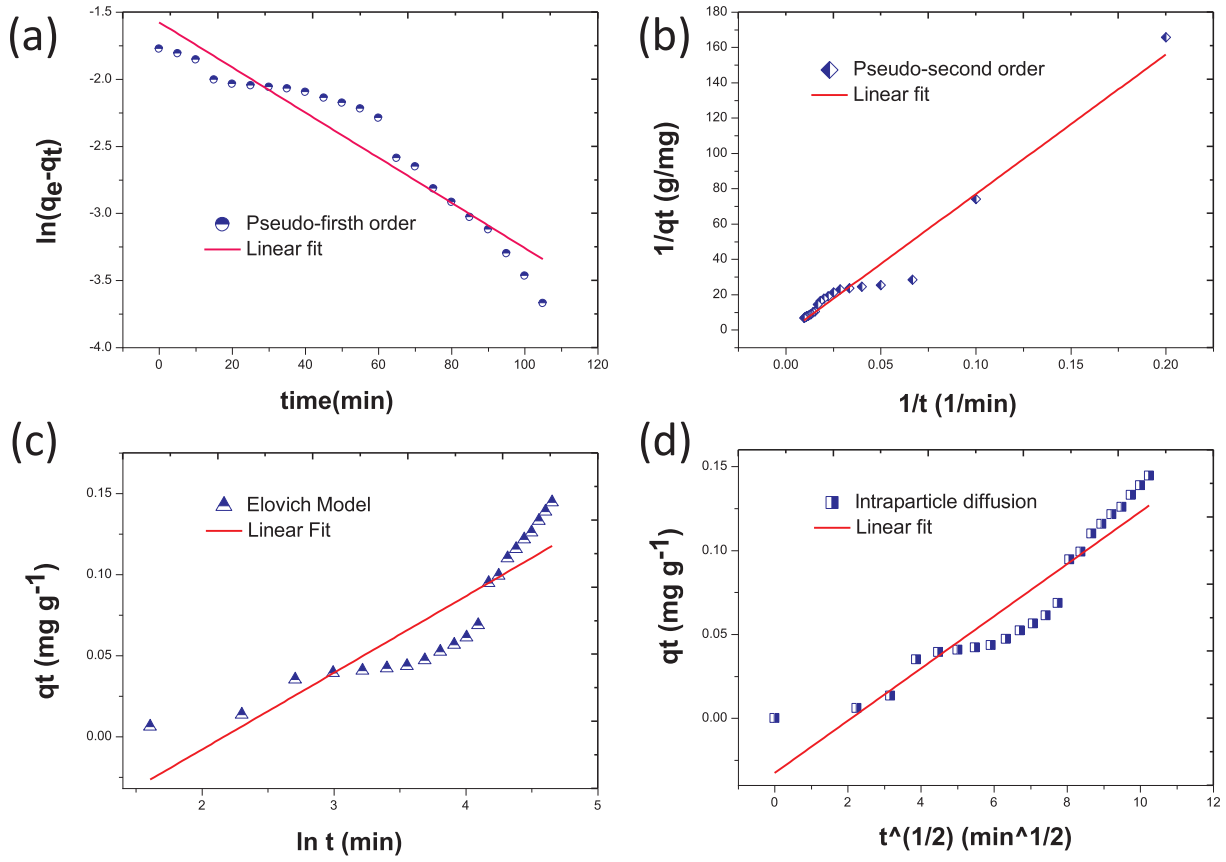

Fig. 9. Kinetic adsorption models (a) Pseudo-first order, (b) Pseudo second order model, (c) Elovich and (d) intraparticle diffusion model.

Table 2
Kinetic parameter calculated from Pseudo first and second order model, the intraparticle diffusion and Elovich model.

Model	Kinetic parameter	
Lagergren first-order K_1 (min^{-1})	K_1	3.63120919
	R^2	0.90796
Pseudo-second order [K2] ($g{\cdot}mg^{-1}{\cdot}min^{-1}$) qe ($mg{\cdot}g^{-1}$)	K_2	0.00617457
	H_2	0.00126455
	qe	0.45254807
	R_2	0.96435
Intraparticle Duffusion Ki ($mg{\cdot}g^{-1}{\cdot}min^{-0.5}$)	C_i	0.03256
	K_i	0.01557
	R^2	0.88554
Elovich α ($mg{\cdot}g^{-1}{\cdot}min$) β ($g{\cdot}mg^{-1}$)	α	2.40962738
	β	0.04733
	R^2	0.79083

calculate for the four models and their respective correlation factor R^2. In this sense, the Pseudo-second order model exhibits the highest value of R^2 (0.975). This value suggests that the MB degradation process follows a kinetic adsorption model of Pseudo second order.

In this regard, several reports indicate that the exchange ionic and chemisorption process are associated to the pseudo-second order model [2]. In this sense, it is possible that the positive partial charges of the Fe_3O_4 can interact with the molecule of the MB. The particle size of the nanoparticle plays a significant role in the degradation process due that the smaller particles sizes promotes a larger potential difference between Fe_3O_4 NPs and MB and hence a higher catalytic activity.

In comparison with other methodologies to obtaining of Fe_3O_4 by green routes, the use of cynara cardunculus offer an efficient green route to obtaining Fe_3O_4 nanoparticles with high crystallinity degree and with homogeneous particle sizes. Is important to note that the particles obtained exhibits a great stability and the agglomerates formation is not observed. Additionally, the kinetic adsorption parameter calculated during the MB degradation process, indicate a competitive behavior respect to the catalytic properties reported for the Fe3O4 nanoparticles [37,38].

Conclusions

The synthesis of Fe3O4 NPs by *cynara cardunculus* was carried out. The antioxidant properties associated to the *cynara cardunculus* have the capacity to reduce the iron ions presents in the precursor solution. Additionally, the PH control of during the synthesis process take also a fundamental role in the iron reduction process. The magnetite structure was fully identified by X-ray diffraction technique and Raman spectroscopy. We can conclude that the synthesis conditions were adequate for the Fe3O4 NPs obtaining. However, the green synthesis by *cynara cardunculus* leaf extract offers an eco-friendly and non-toxic alternative to obtaining Fe3O4 NPs. On the other hand, the Fe_3O_4 NPs obtained shows a catalytic activity in the methylene blue degradation process. The MB degradation rate and the kinetic adsorption behavior is governed by the Pseudo- second order model (type 2) which describe an exchange ionic and chemisorption process between the positive partial charges of the Fe_3O_4 NPs and the molecule of the MB. Given has result the decomposition of the MB molecule and consequently the MB degradation. Finally, we can affirm that the Fe_3O_4 NPs synthetized by *cynara cardunculus* leaf extract have potential catalytic applications, particularly for water remediation containing this kind of organic dyes.

Conflict of interest

On behalf of all authors, the corresponding author states that there

is no conflict of interest.

Acknowledgment

Álvaro de Jesús Ruíz-Baltazar appreciates the support provided by the "Centro de Física Aplicada y Tecnología Avanzada" (National Materials Characterization Laboratory) in collaboration with CONACYT through "Cátedras CONACYT" program.

References

[1] Chen P, Li H, Song S, Weng X, He D, Zhao Y. Adsorption of dodecylamine hydrochloride on graphene oxide in water. Results Phys 2017;7:2281–8. https://doi.org/10.1016/j.rinp.2017.06.054.
[2] de Jesús Ruíz-Baltazar Á, Reyes-López SY, Pérez R. Magnetic structures synthesized by controlled oxidative etching: structural characterization and magnetic behavior. Results Phys 2017;7:1828–32. https://doi.org/10.1016/j.rinp.2017.05.001.
[3] Baskakov AO, Solov'eva AY, Ioni YV, Starchikov SS, Lyubutin IS, Khodos II, Avilov AS, Gubin SP. Magnetic and interface properties of the core-shell Fe3O4/Au nanocomposites. Appl Surf Sci 2017;422:638–44. https://doi.org/10.1016/j.apsusc.2017.06.029.
[4] Mohammadiyan E, Ghafuri H, Kakanejadifard A. Synthesis and characterization of a magnetic Fe3O4@CeO2nanocomposite decorated with Ag nanoparticle and investigation of synergistic effects of Ag on photocatalytic activity. Optik (Stuttg) 2018;166:39–48. https://doi.org/10.1016/j.ijleo.2018.03.044.
[5] Hou X, Wang X, Mi W. Progress in Fe3O4-based multiferroic heterostructures. J Alloys Compd 2018;765:1127–38. https://doi.org/10.1016/j.jallcom.2018.06.287.
[6] Prasankumar T, Wiston BR, Gautam CR, Ilangovan R, Jose SP. Synthesis and enhanced electrochemical performance of PANI/Fe3O4nanocomposite as supercapacitor electrode. J Alloys Compd 2018;757:466–75. https://doi.org/10.1016/j.jallcom.2018.05.108.
[7] Xia Q, Jiang Z, Li D, Wang J, Yao Z. Green synthesis of a dendritic Fe3O4@Feocomposite modified with polar C-groups for Fenton-like oxidation of phenol. J Alloys Compd 2018;746:453–61. https://doi.org/10.1016/j.jallcom.2018.02.311.
[8] Alvarez RAB, Cortez-Valadez M, Bueno LON, Britto Hurtado R, Rocha-Rocha O, Delgado-Beleño Y, Martinez-Nuñez CE, Serrano-Corrales LI, Arizpe-Chávez H, Flores-Acosta M. Vibrational properties of gold nanoparticles obtained by green synthesis. Phys E Low-Dim Syst Nanostruct 2016;84:191–5. https://doi.org/10.1016/j.physe.2016.04.024.
[9] Pan Y, Zeng W, Li L, Zhang Y, Dong Y, Ye K, et al. Surfactant assisted, one-step synthesis of Fe3O4nanospheres and further modified Fe3O4/C with excellent lithium storage performance. J Electroanal Chem 2018;810:248–54. https://doi.org/10.1016/j.jelechem.2018.01.025.
[10] Nayamadi Mahmoodabadi A, Kompany A, Mashreghi M. Characterization antibacterial and cytotoxicity studies of graphene-Fe3O4nanocomposites and Fe3O4nanoparticles synthesized by a facile solvothermal method. Mater Chem Phys 2018;213:285–94. https://doi.org/10.1016/j.matchemphys.2018.04.033.
[11] Yingzhe Z, Yuxing H, Qingdong Q, Fuchun W, Wankun W, Yongmei L. The synthesis of Cu/Fe/Fe3O4 catalyst through the aqueous solution ball milling method assisted by high-frequency electromagnetic field. Superlatt Microstruct 2018;118:123–9. https://doi.org/10.1016/j.spmi.2018.04.016.
[12] Xiang Z, Song Y, Xiong J, Pan Z, Wang X, Liu L, et al. Enhanced electromagnetic wave absorption of nanoporous Fe3O4 @ carbon composites derived from metal-organic frameworks. Carbon N Y 2019;142:20–31. https://doi.org/10.1016/j.carbon.2018.10.014.
[13] Madhuvilakku R, Alagar S, Mariappan R, Piraman S. Green one-pot synthesis of flowers-like Fe3O4/rGO hybrid nanocomposites for effective electrochemical detection of riboflavin and low-cost supercapacitor applications. Sens Actuat, B Chem 2017;253:879–92. https://doi.org/10.1016/j.snb.2017.06.126.
[14] Krishna R, Dias C, Ventura J, Titus E. Green and facile decoration of Fe3O4nanoparticles on reduced graphene oxide. Mater Today Proc 2016;3:2807–13. https://doi.org/10.1016/j.matpr.2016.06.030.
[15] Cheera P, Karlapudi S, Sellola G, Ponneri V. A facile green synthesis of spherical Fe3O4magnetic nanoparticles and their effect on degradation of methylene blue in aqueous solution. J Mol Liq 2016;221:993–8. https://doi.org/10.1016/j.molliq.2016.06.006.
[16] Sajjadi M, Nasrollahzadeh M, Mohammad Sajadi S. Green synthesis of Ag/Fe3O4nanocomposite using Euphorbia peplus Linn leaf extract and evaluation of its catalytic activity. J Colloid Interf Sci 2017;497:1–13. https://doi.org/10.1016/j.jcis.2017.02.037.
[17] de Jesús Ruíz-Baltazar Á, Reyes-López SY, Larrañaga D, Estévez M, Pérez R. Green synthesis of silver nanoparticles using a Melissa officinalis leaf extract with antibacterial properties. Results Phys 2017;7. https://doi.org/10.1016/j.rinp.2017.07.044.
[18] Singh KK, Senapati KK, Sarma KC. Synthesis of superparamagnetic Fe3O4nanoparticles coated with green tea polyphenols and their use for removal of dye pollutant from aqueous solution. J Environ Chem Eng 2017;5:2214–21. https://doi.org/10.1016/j.jece.2017.04.022.
[19] Najafinejad MS, Mohammadi P, Mehdi Afsahi M, Sheibani H. Green synthesis of the Fe3O4@polythiophen-Ag magnetic nanocatalyst using grapefruit peel extract: application of the catalyst for reduction of organic dyes in water. J Mol Liq 2018;262:248–54. https://doi.org/10.1016/j.molliq.2018.04.052.
[20] Atla SB, Lin WR, Chien TC, Tseng MJ, Shu JC, Chen CC, et al. Fabrication of Fe3O4/ZnO magnetite core shell and its application in photocatalysis using sunlight. Mater Chem Phys 2018;216:380–6. https://doi.org/10.1016/j.matchemphys.2018.06.020.
[21] Moradi L, Tadayon M. Green synthesis of 3,4-dihydropyrimidinones using nano Fe3O4@meglumine sulfonic acid as a new efficient solid acid catalyst under microwave irradiation. J Saudi Chem Soc 2017;22:66–75. https://doi.org/10.1016/j.jscs.2017.07.004.
[22] Madhuvilakku R, Alagar S, Mariappan R, Piraman S. Green one-pot synthesis of flowers-like Fe3O4/rGO hybrid nanocomposites for effective electrochemical detection of riboflavin and low-cost supercapacitor applications. Sens Actuat B Chem 2017. https://doi.org/10.1016/j.snb.2017.06.126.
[23] Moradi L, Tadayon M. Green synthesis of 3,4-dihydropyrimidinones using nano Fe3O4@meglumine sulfonic acid as a new efficient solid acid catalyst under microwave irradiation. J Saudi Chem Soc 2017. https://doi.org/10.1016/j.jscs.2017.07.004.
[24] de Falco B, Incerti G, Amato M, Lanzotti V. Artichoke: botanical, agronomical, phytochemical, and pharmacological overview. Phytochem Rev 2015;14:993–1018. https://doi.org/10.1007/s11101-015-9428-y.
[25] Ruíz-Baltazar ÁDJ, Reyes-López SY, Mondragón-Sánchez MDL, Estevez M, Hernández-Martinez AR, Pérez R. Biosynthesis of Ag nanoparticles using cynara cardunculus leaf extract: evaluation of their antibacterial and electrochemical activity. Results Phys 2018;11:1142–9. https://doi.org/10.1016/j.rinp.2018.11.032.
[26] Ruíz-baltazar A, Esparza R, Rosas G, Pérez R. Effect of the surfactant on the growth and oxidation of iron nanoparticles. J Nanomater 2015;2015.
[27] Wei Y, Han B, Hu X, Lin Y, Wang X, Deng X. Synthesis of Fe3O4 nanoparticles and their magnetic properties. Procedia Eng 2012;27:632–7. https://doi.org/10.1016/j.proeng.2011.12.498.
[28] Jubb AM, Allen HC. Vibrational spectroscopic characterization of hematite, maghemite, and magnetite thin films produced by vapor deposition. ACS Appl Mater Interf 2010;2:2804–12. https://doi.org/10.1021/am1004943.
[29] Soares PIP, Alves AMR, Pereira LCJ, Coutinho JT, Ferreira IMM, Novo CMM, et al. Effects of surfactants on the magnetic properties of iron oxide colloids. J. Colloid Interf Sci 2014;419:46–51. https://doi.org/10.1016/j.jcis.2013.12.045.
[30] Ruíz-Baltazar A, Esparza R, Rosas G, Pérez R. Effect of the surfactant on the growth and oxidation of iron nanoparticles. J Nanomater 2015;2015. https://doi.org/10.1155/2015/240948.
[31] Srivastava M, Kumar B, Prasad R, Kumari N, Prasad SN. Spectral studies of some transition metal chelates with thiolactic anilide and thiolactic-p-toluidide, Part-II. Asian J Chem 1999;11:1501–4. https://doi.org/10.1002/jrs.
[32] Ho YS. Isotherms for the sorption of lead onto peat: Comparison of linear and non-linear methods. Polish J Environ Stud 2006;15:81–6. https://doi.org/10.1016/j.watres.2005.10.040.
[33] Ruíz-baltazar A, Pérez R. Kinetic adsorption study of silver nanoparticles on natural zeolite: experimental and theoretical models. Appl Sci 2015:1869–81. https://doi.org/10.3390/app5041869.
[34] Ruíz-baltazar A, Esparza R, Gonzalez M, Rosas G, Pérez R. Preparation and characterization of natural zeolite modified with iron nanoparticles. J Nanomater 2015;2015:1–9.
[35] Soria-serna LA, Torres-pérez J, Reyes-lópez SY. Tetracycline adsorption on steam alternative activated carbon: kinetic and thermodynamic parameters. Desalin Water Treat 2018;114:307–19. https://doi.org/10.5004/dwt.2018.22313.
[36] Roque-Ruiz JH, Medellín-Castillo NA, Reyes-López SY. Fabrication of α-alumina fibers by sol-gel and electrospinning of aluminum nitrate precursor solutions. Results Phys 2019;12:193–204. https://doi.org/10.1016/j.rinp.2018.11.068.
[37] Cheera P, Karlapudi S, Sellola G, Ponneri V. A facile green synthesis of spherical Fe3O4magnetic nanoparticles and their effect on degradation of methylene blue in aqueous solution. J Mol Liq 2016. https://doi.org/10.1016/j.molliq.2016.06.006.
[38] Bishnoi S, Kumar A, Selvaraj R. Facile synthesis of magnetic iron oxide nanoparticles using inedible cynometra ramiflora fruit extract waste and their photocatalytic degradation of methylene blue dye. Mater Res Bull 2018;97:121–7. https://doi.org/10.1016/j.materresbull.2017.08.040.